Available online at www.sciencedirect.com
ScienceDirect
Journal of Luminescence 127 (2007) 397–403
JOURNAL OF LUMINESCENCE
www.elsevier.com/locate/jlumin

Luminescence and excitation spectra of YAG:Nd^{3+} excited by synchrotron radiation

Lixin Ning[a], Peter A. Tanner[a,*], Vachagan V. Harutunyan[b], Eduard Aleksanyan[b], Vladimir N. Makhov[c,d], Marco Kirm[d]

[a]*Department of Biology and Chemistry, City University of Hong Kong, Tat Chee Avenue, Kowloon, Hong Kong S.A.R., PR China*
[b]*Yerevan Physics Institute, 2 Alikhanian Brothers Str., 375036 Yerevan, Armenia*
[c]*Lebedev Physical Institute, Leninskii Prospect 53, 119991 Moscow, Russia*
[d]*Institute of Physics, University of Tartu, Riia 142, 51014 Tartu, Estonia*

Received 19 October 2006; received in revised form 12 January 2007; accepted 24 January 2007
Available online 15 February 2007

Abstract

The low-temperature $4f^25d \rightarrow 4f^3$ fast emission of Nd^{3+} from YAG:Nd^{3+} has been studied under excitation by synchrotron radiation. Additionally, $4f^3 \rightarrow 4f^3$ luminescence of Nd^{3+} has been observed and assigned to transitions from the $^2F(2)_{5/2}$ and $^4F_{3/2}$ multiplet terms. The observed experimental spectra of Nd^{3+} d–f emission and f–d excitation are well simulated by crystal-field calculations.

PACS: 33.50.Dq; 33.70.−w; 42.62.Fi; 71.70.Ch; 78.55.Hx

Keywords: d–f Transition; Fast UV luminescence of Nd^{3+}; Crystal-field calculation; Excitation spectra; Vacuum ultraviolet

1. Introduction

The vacuum ultraviolet emission and excitation spectra of Nd^{3+} diluted into wide band gap hosts have recently attracted attention for applications such as laser crystals [1], scintillators [2,3], upconverters [4,5], as well as for theoretical investigations [6,7]. The typical $4f^25d^1 \rightarrow 4f^3$ luminescence of Nd^{3+} in various oxide and fluoride hosts is fast (with a decay time of the order 10 ns described by a single exponential) and shows usually a broad-band emission with the shortest wavelength and strongest band centered around 190 nm. This band is assigned to the parity and spin-allowed transitions from the lowest $4f^25d^1$ crystal-field level(s) to the ^4I_J ($2J = 9, 11, 13, 15$) ground multiplet terms of Nd^{3+}. Although a variety of wide band oxide and fluoride hosts have been doped with Nd^{3+} and employed in these investigations, we are unaware of studies of d–f emission and f–d excitation spectra of Nd^{3+} doped into the well-known laser host $Y_3Al_{12}O_5$ (YAG). The only exception is the investigation of the Nd^{3+} $4f^3 \rightarrow 4f^25d$ absorption for YAG:Nd^{3+} reported in Ref. [8]. In a view of the importance of this material for practical applications, we have undertaken experimental and theoretical investigations of the low-temperature emission and excitation spectra of Nd^{3+}-doped YAG (including the comparison with an undoped YAG crystal) in the ultraviolet and vacuum ultraviolet spectral regions. We benefit from previous thorough studies of the optical phonons of the YAG host [9] and of the $4f^3$ energy levels of Nd^{3+} in this host lattice, which have been fitted by crystal-field calculations [10,11]. In order to guide the reader, the schematic diagram of the $4f^3$ and $4f^25d$ energy levels of Nd^{3+} in YAG:Nd^{3+} are shown in Fig. 1, in comparison with the conduction band of the host lattice.

2. Experimental methods

The nominally pure YAG crystal and YAG crystals doped with Nd^{3+} (0.5 and 1.0 at%) were grown by the Czochralski method. Low-temperature (~10 K) emission (200–1000 nm) and excitation (50–300 nm) spectra of the

*Corresponding author. Tel.: +852 2788 7840; fax: +852 2788 7406.
E-mail address: bhtan@cityu.edu.hk (P.A. Tanner).

0022-2313/$ - see front matter © 2007 Elsevier B.V. All rights reserved.
doi:10.1016/j.jlumin.2007.01.019

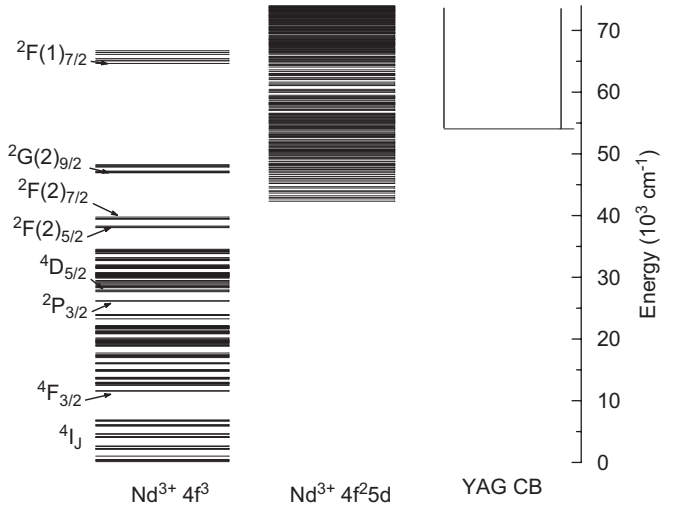

Fig. 1. Schematic $4f^3$ and $4f^25d$ energy levels of Nd^{3+} in YAG:Nd^{3+} up to 75,000 cm^{-1} and comparison with the host band gap.

samples were measured at the SUPERLUMI station [12] of HASYLAB at DESY (Hamburg) using synchrotron radiation from the DORIS storage ring. Time-integrated emission spectra were recorded with a 0.3 m Czerny–Turner-type imaging monochromator-spectrograph SpectraPro-308i (Acton Research Corporation) equipped with a liquid nitrogen cooled CCD detector (Princeton Instruments Inc.). The spectral resolution of the analyzing monochromator with the 300 lines mm^{-1} grating was set to ~0.5 nm. Emission spectra in the deep UV region (260–330 nm) were measured with the increased spectral resolution ~0.25 nm using the 1200 lines mm^{-1} grating. Excitation spectra were recorded with an instrumental resolution of primary monochromator ~0.3 nm by using a photomultiplier tube (Hamamatsu R6358P) installed in another arm of the analyzing monochromator. Time-resolved emission spectra were recorded using the same PMT with quite a moderate spectral resolution of the analyzing monochromator ~10 nm in order to produce luminescence spectra of sufficient quality. The crystals were cleaved prior to the mounting onto a copper sample holder attached to cold finger of a flow-type liquid helium cryostat (Cryovac GmbH).

3. Results and discussion

3.1. Calculation of $4f^25d$ energy levels

The YAG crystal has a bcc structure (space group Ia3d or O_h^{10}, $Z = 230$ [13]). The Nd^{3+} ion occupies the 24(c) sites of Y^{3+} with D_2 point symmetry, and each of the ions is dodecahedrally coordinated to eight O. The crystal-field parameters B_q^k for the D_2 point symmetry relevant in the $4f^25d$ energy level calculations are those with $k = 2, 4, 6$, and $q = 0, 2, 4, 6$ with $q \leqslant k$. The energy level calculations employed the extended f-shell programs of Prof. M.F. Reid, in which the electronic levels were calculated by simultaneous diagonalization of various parameterized Hamiltonians for $4f^3$ and $4f^25d$ configurations of Nd^{3+} in YAG. A detailed description of the parameterized Hamiltonians and the calculations can be found in Ref. [14]. In the calculation of $4f^25d$ energy levels, parametric values for the interactions of the $4f^2$ core, including Coulomb interaction between the 4f electrons, spin–orbit interaction, other smaller atomic interactions, and the crystal-field interaction, were taken from those of $4f^3$ ground configuration, and have been determined from the fits of the experimentally observed $4f^3$ energy levels of Nd^{3+} in YAG [11]. The spin–orbit parameter for the 5d electron in the $4f^25d$ configuration was calculated using a standard atomic computer program [15]. The five crystal-field parameters of the 5d electron, B_0^2(dd), B_2^2(dd), B_0^4(dd), B_2^4(dd), and B_4^4(dd), were derived from optimization with respect to four of the total of five experimental 5d levels of Ce^{3+} in YAG [16]. The experimental Ce^{3+} level at ~38,000 cm^{-1} (265 nm) was removed due to uncertainty of its assignment. In the optimization, the ratio $B_2^2(\mathrm{dd})/B_0^2(\mathrm{dd})$ was fixed to the value for the $4f^3$ electrons of Nd^{3+} in YAG [11]; hence a total of four parameters were freely varied within certain allowed ranges, with the signs being kept the same as of the corresponding 4f parameters. The 5d spin–orbit parameter was fixed to the value (991 cm^{-1}) for Ce^{3+} calculated with the standard atomic computer program, and the four parameters were freely varied within certain allowed ranges with the same signs as the corresponding 4f parameters of Nd^{3+} in YAG [11], and optimized by repeatedly calculating the 5d levels until the best agreement was obtained between the four calculated and observed crystal-field levels. The calculated 5d electronic energies (with respect to the lowest one) were finally derived as [calcd (exptl)]: 0 (0) cm^{-1}, 7581 (7582) cm^{-1}, 22,505 (22,503) cm^{-1}, 24,760 (–) cm^{-1}, 27,019 (27,020) cm^{-1}, where the experimental values were measured from the observed $4f \rightarrow 5d$ absorption band positions of Ce^{3+} in YAG [16]. The f–d interaction parameters were estimated using the standard atomic computer program [15] but were reduced to 74% of the calculated free-ion values [17,18]. In addition, the Δ_E(fd) parameter, which accounts for the difference between the average energies of $4f^25d$ and $4f^3$ configurations, was adjusted to obtain the best agreement between experiment and calculation. The energy parameters used in the calculation of the $4f^25d$ energy levels are collected in Table 1.

3.2. Calculation of $4f^3$–$4f^25d$ transition intensities

The transitions between $4f^3$ and $4f^25d$ states are electric dipole allowed. Because the 5d orbital is more extended than the 4f orbital, there is a displacement of the equilibrium position of the ligands in the $4f^25d$ excited states, and thus most of the transition intensity is located in a broad vibronic band. We approximate here that the unpolarized intensity I_{if} of the vibronic band is

Table 1
Energy parameters for $4f^25d$ configuration of Nd^{3+} in YAG

Parameter	cm^{-1}	Parameter	cm^{-1}
F^2(ff)	70,845	B_2^6(ff)	−390
F^4(ff)	51,235	B_4^6(ff)	1610
F^6(ff)	34,717	B_6^6(ff)	−281
ζ(ff)	876	ζ(dd)	1132
α(ff)	21.1	B_0^2(dd)	−7665
β(ff)	−645	B_2^2(dd)	4908
γ(ff)	1660	B_0^4(dd)	−49,379
M^0(ff)[a]	1.62	B_2^4(dd)	3069
P^2(ff)[a]	107	B_4^4(dd)	21,440
B_0^2(ff)	−405	Δ_E(fd)	47,889
B_2^2(ff)	179	F^2(fd)	22,626
B_0^4(ff)	−2823	F^4(fd)	11,205
B_2^4(ff)	540	G^1(fd)	9787
B_4^4(ff)	1239	G^3(fd)	8306
B_0^6(ff)	955	G^5(fd)	6437

Parameters for the splitting of $4f^2$ core were taken from those of $4f^3$ configuration [11]. The spin–orbit parameter of the 5d electron was calculated using Cowan's code [15] and the crystal-field parameters were obtained by fitting the experimental 5d crystal-field levels of Ce^{3+} in YAG [16]. The f–d interaction parameters were also calculated using Cowan's code [15], but reduced by 26%.

[a] $M^2(\text{ff}) = 0.558\ M^0(\text{ff})$, $M^4(\text{ff}) = 0.377\ M^0(\text{ff})$; $P^4(\text{ff}) = 0.75\ P^2(\text{ff})$, $P^6(\text{ff}) = 0.50\ P^2(\text{ff})$.

proportional to the electric dipole transition line strength between the relevant initial $4f^3$ level $|f^3\Gamma_i\rangle$ and the final $|f^2d\Gamma_f\rangle$ level, multiplied by the transition wavenumber $\bar{v}_{if}$ of the zero-phonon line

$$I_{if} \propto \bar{v}_{if} \sum_{q,\gamma_i,\gamma_f} \left|\left\langle f^3\Gamma_i\gamma_i \middle| D_q^1 \middle| f^2 d\Gamma_f\gamma_f \right\rangle\right|^2, \quad (1)$$

where D_q^1 is the electric dipole operator, and the summation is over the polarization q ($q = 0, \pm 1$) and the components γ of the initial and final levels. The electric dipole matrix element in Eq. (1) can be calculated with the pure electronic wave functions obtained from the energy level calculations for $4f^3$ and $4f^25d$ configurations, and the formulae may be found in Ref. [19]. Since there are many vibrational modes for the YAG crystal [9], the spectra contain the superposition of a number of vibrational progressions, giving rather featureless vibronic bands. Thus, no attempts have been made to simulate the spectra by assuming a Gaussian band superimposed on each zero-phonon line.

3.3. Emission and excitation spectra of pure YAG

The optical spectra of pure YAG have been thoroughly studied before in a wide spectral range and a steeply rising intrinsic absorption edge has been found near 6.7 eV [8]. Fig. 2 shows the emission and excitation spectra of pure YAG at 8.5 K. The 6.9 eV (180 nm) excited emission from pure YAG comprises a broad nonelementary band centered near 4.67 eV (265 nm), which consists of several

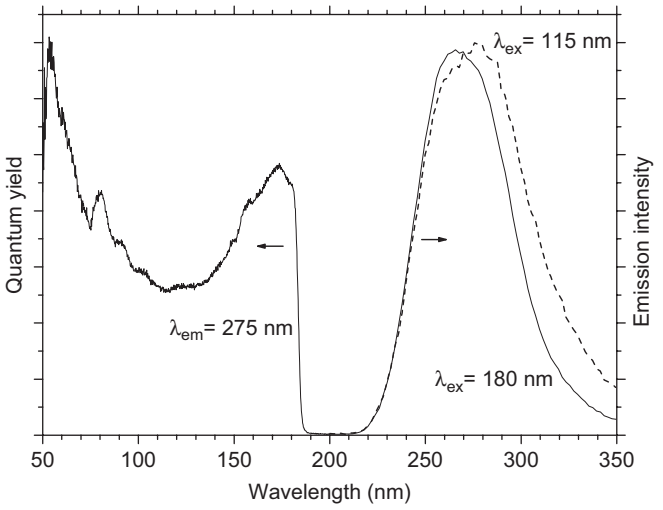

Fig. 2. Emission spectra excited at 180 nm (solid curve) and 115 nm (dashed curve) and excitation spectrum of 275 nm emission of pure YAG at 8.5 K.

overlapping bands, the most intense of them being centered at 4.1, 4.3, and 4.75 eV. At 10 K this emission has slow decay, which is longer than the detection limit of the used set-up ~1 μs. The excitation spectrum of this intrinsic emission shows a threshold at ~6.7 eV (185 nm) and a first maximum at ~7.15 eV (173 nm). The Stokes shift between the maxima of the emission and excitation spectra is ~2.5 eV. Obviously, the excitation threshold corresponds to the edge of intrinsic (excitonic) absorption of the host. The efficiency of excitation of this intrinsic emission is rather high also in the whole region of band-to-band transitions (E_g in YAG is ~8.0 eV [20]). The intrinsic luminescence of YAG is usually interpreted as being due to superposition of luminescence from self-trapped excitons (STEs) localized both at regular sites and near different defects of the lattice. Generally, our results on intrinsic emission of pure YAG are in good agreement with those obtained earlier [20,21]. The emission spectrum looks remarkably broadened compared to the excitonic excitation region. One explanation is because of the much higher relative intensity of the lowest-energy sub-band at 4.1 eV being effectively excited via the electron–hole mechanism. A referee has given an alternative explanation that the absorption transition involves band states with almost no lattice relaxation, whereas the emission comes from the relaxed state of a different equilibrium position than the ground state.

3.4. $4f^3$–$4f^3$ emission spectra of YAG:Nd^{3+}

Emission from the lowest level of the $4f^3\ ^2F(2)_{5/2}$ multiplet (at 37,777 cm^{-1}) has been detected under the synchrotron radiation excitation ($\lambda_{ex} = 192$ nm) into the $4f^25d$ configuration (Fig. 3). As subsequently discussed, the lowest $4f^25d$ crystal-field level in YAG:Nd^{3+} is assigned at 42,362 cm^{-1} from our experimental data. After the 192 nm

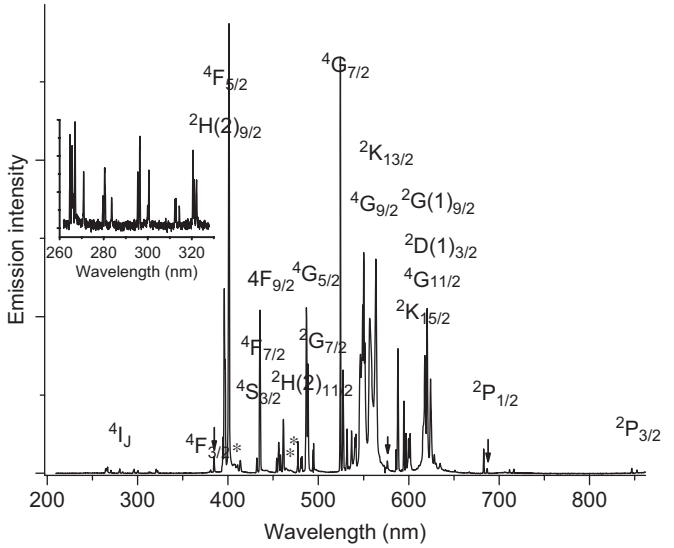

Fig. 3. 192 nm excited luminescence spectrum of YAG:Nd^{3+} (0.5 at%) at 8.5 K between 200 and 860 nm. The luminescent multiplet term is $^2F(2)_{5/2}$ and the terminal multiplets are labeled. The starred bands are vibronic structure. The arrows point to (from left to right) second and third order excitation lines and to the Cr^{3+} R1 line.

(~52,080 cm^{-1}) excitation radiation is absorbed by the crystal, the nonradiative relaxation occurs to this lowest 5d-level, which then populates the $4f^3$ multiplet $^2F(2)_{7/2}$ (located between 39,202 and 39,690 cm^{-1} [11]). Since the energy gap between this multiplet and the lowest $4f^25d$ level is small enough ~2670 cm^{-1}, i.e. not more than 4 phonon energies, the nonradiative decay from the $4f^25d$ level is the dominant process in YAG:Nd^{3+}. However, as it will be shown below, the radiative decay of the Nd^{3+} $4f^25d$ level is also observed in YAG:Nd^{3+} at low temperature. The $^2F(2)_{7/2}$ multiplet (Fig. 1) also decays nonradiatively populating the luminescent multiplet term $^2F(2)_{5/2}$ (located between 37,777 and 38,192 cm^{-1}) which is in turn located at ~3380 cm^{-1} (i.e. 4–5 phonons) above the next lowest crystal-field level. In summary, the appearance of strong $^2F(2)_{5/2}$ emission is due to efficient nonradiative cascade relaxation to this level from the lowest level of the $4f^25d$ configuration.

As shown in Fig. 3, the 18 spectral lines combined into four groups were resolved in the spectral range between 265 and 333 nm (inset of Fig. 3), which correspond to the observed weak transitions to the ground ^4I_J multiplet, and many strong overlapping lines were detected in the region 390–720 nm, which correspond to transitions from the lowest level of the $^2F(2)_{5/2}$ multiplet to many other levels of the $4f^3$ configuration. The terminal multiplet terms are marked in the figure. We have analyzed the derived energies of the terminal crystal-field states against the experimental energies in the tabulation of Burdick et al. [11] and the overall agreement is good. In some cases, such as for the transitions from $^2F(2)_{5/2}$ to ^4I_J, (shown as the upper left hand inset in Fig. 3), some transitions overlap and are not well separated by resolution applied in the ultraviolet spectral region. The spectra recorded in the visible and near-infrared regions are more clearly resolved, however, and from the bands in the spectral region near 630 nm, we are able to reassign levels 94 and 95 of YAG:Nd^{3+} in the experimental energy tabulation of Burdick et al. [11] at 21,870 and 21,904 cm^{-1}, respectively. These energies are in good agreement with the energies from our $4f^3$ crystal-field calculation (21,871, 21,906 cm^{-1}). Three fairly weak broad bands in Fig. 3 are marked by asterisks. These correspond to vibronic structures with the derived energies of 373 cm^{-1} (a_{1g} phonon) [9] in each case. Thus, all of the bands in Fig. 3 correspond to emission from $^2F(2)_{5/2}$, with three exceptions which are marked by vertical arrows. The two higher energy features correspond to the second and third order of synchrotron radiation excitation applied. There is only one crystal-field level associated with $^2P_{1/2}$ (at 23,148 cm^{-1}) and the transition from $^2F(2)_{5/2}$ is located near 683 nm and marked in Fig. 3. The "additional" weak band just at lower energy (~686 nm, under the vertical arrow) most likely arises from the R1 line of the Cr^{3+} impurity [22].

Fig. 4 shows the lower energy region between 860 and 975 nm of the 192-nm-excited spectrum, which corresponds to the $^4F_{3/2} \rightarrow {}^4I_{9/2}$ emission. The spectrum consists of 5 lines arising from the transitions to 5 crystal-field levels of the $^4I_{9/2}$ multiplet and the derived energies are marked. Under 175 nm excitation, the $4f^3$–$4f^3$ emission spectrum is similar to that shown in Fig. 3, except that an additional broad emission band is observed which peaks at ~263 nm (4.7 eV). It is the intrinsic STE emission, as in pure YAG, but the width of this band is much reduced because of the absence of contribution of the lower-energy (4.1 eV) emission.

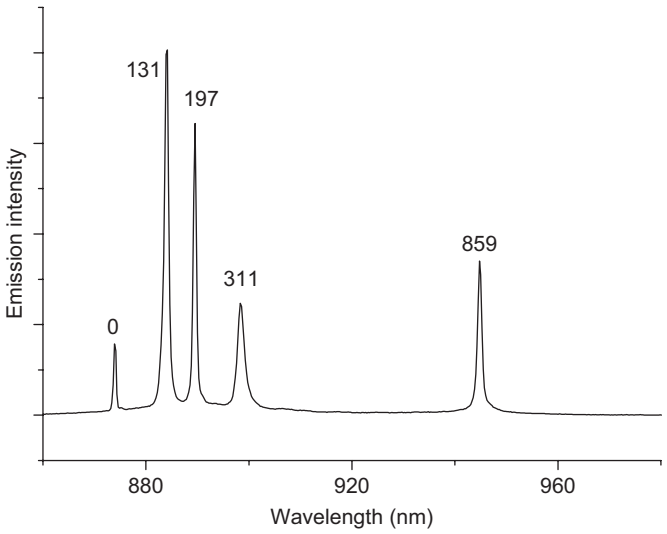

Fig. 4. 192 nm excited luminescence spectrum of YAG:Nd^{3+} (0.5 at%) at 8.5 K between 860 and 975 nm. The transitions correspond to $^4F_{3/2} \rightarrow {}^4I_{9/2}$ and the derived crystal-field level energies of the ground state multiplet term are marked.

3.5. 5d–4f emission and excitation spectra of YAG:Nd^{3+}

The measurements of time-resolved emission spectra from Nd^{3+}-doped YAG under excitation in the region of the $4f^3 \rightarrow 4f^2 5d$ transitions in Nd^{3+} revealed the presence of the rather weak, but fast emission with the main broad band peaking at 248 nm (5.0 eV) and an even lower intensity band at ~350 nm (3.55 eV), as shown by the dotted curve in Fig. 5. Experimental conditions (strong increase of Nd^{3+} f–f emission as well as of scattered light from the second order of exciting radiation) prohibited measurements of time-resolved emission spectrum at wavelengths longer than ~370 nm. The characteristic decay time of this broad-band emission is ~2 ns. This emission is ascribed to interconfigurational $4f^2 5d \rightarrow 4f^3$ radiative transitions in YAG:Nd^{3+} from the lowest level of the $4f^2 5d$ configuration. The rather short decay time of this emission indicates the presence of efficient nonradiative decay channels depopulating the $4f^2 5d$ level of Nd^{3+} in YAG:Nd^{3+}.

The $4f^2 5d \rightarrow 4f^3$ emission spectrum of YAG:Nd^{3+} was calculated using the same procedure as described above in Section 3.2 for the $4f^3 \rightarrow 4f^2 5d$ excitation spectrum, except that in Eq. (1) initial and final electronic levels are now of the $4f^2 5d$ and $4f^3$ configurations, respectively, with the factor $\bar{v}_{if}$ replaced by $\bar{v}_{if}^3$. The lowest $4f^2 5d$ crystal-field level is of spin quartet character so that the transition to ^4I_J is spin allowed. The orbital multiplet parentage is however rather mixed, with the appreciable contributions of $^4I_{9/2}$, $^4G_{5/2}$, and $^4K_{11/2}$ states. The calculated positions and relative emission intensities from this lowest $4f^2 5d$ energy level to the crystal-field levels of $4f^3$ are shown as vertical bars in Fig. 5, and it is clear that the calculated intensity resides in the transitions to the ^4I_J, ^4F_J, and ^4G_J multiplets. This is in contrast to the $4f^2 5d \rightarrow 4f^3$ emission of Nd^{3+} in Cs_2NaYF_6, in which almost all of the intensity is concentrated in transitions to the ^4I_J multiplets [17].

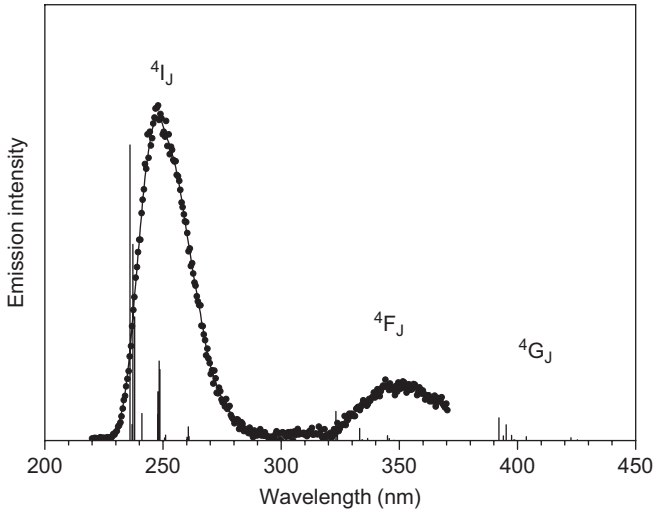

Fig. 5. Luminescence spectrum of 192 nm excited fast emission component from YAG:Nd^{3+} (0.5 at%) at 10 K. The vertical bars indicate the calculated $4f^2 5d \rightarrow 4f^3$ emission line positions and intensities. The terminal $4f^3$ multiplets are marked.

The excitation spectrum of this fast emission coincides with that of the Nd^{3+} 4f–4f emission, as shown in Fig. 6. Low-intensity sharp features between 37,700 and 40,000 cm^{-1} correspond to absorptions by $^2F(2)_{5/2}$ and $^2F(2)_{7/2}$ crystal-field states. The excitation spectra show a distinct onset at ~237 nm corresponding to the edge of the $4f^3 \rightarrow 4f^2 5d$ interconfigurational transitions in Nd^{3+}. From the short-wavelength side, these transitions are obviously modulated by the edge of strong intrinsic absorption of the host at ~185 nm. A rather rich structure is observed in the excitation spectrum of Nd^{3+} 4f–4f emission at 400 nm of YAG:Nd^{3+} recorded with higher resolution (Fig. 7). A well-resolved sharp line at 236.1 nm (42,362 cm^{-1}) observed at the edge of the excitation spectrum is assigned to a $4f^3 \rightarrow 4f^2 5d$ zero-phonon line, with a further partially resolved band to higher energy representing the first member of the vibrational progression upon this origin in the ~370 cm^{-1} a_{1g} mode (these bands are marked by vertical arrows in Fig. 7). There is also a band at ~200 cm^{-1} above this zero-phonon line (also marked by a vertical dashed arrow in Fig. 7), the origin of which could be purely electronic or vibronic. This question is still left open for further experiments. We were not able to resolve any fine structure (if present) in the Nd^{3+} $4f^2 5d \rightarrow 4f^3$ emission spectrum because time-resolved spectra could be measured only with quite a moderate spectral resolution due to low-emission intensity.

In Fig. 6, the calculated positions and intensities of transitions from the $4f^3$ ground state level to the $4f^2 5d$ crystal-field levels are shown as vertical bars. The main

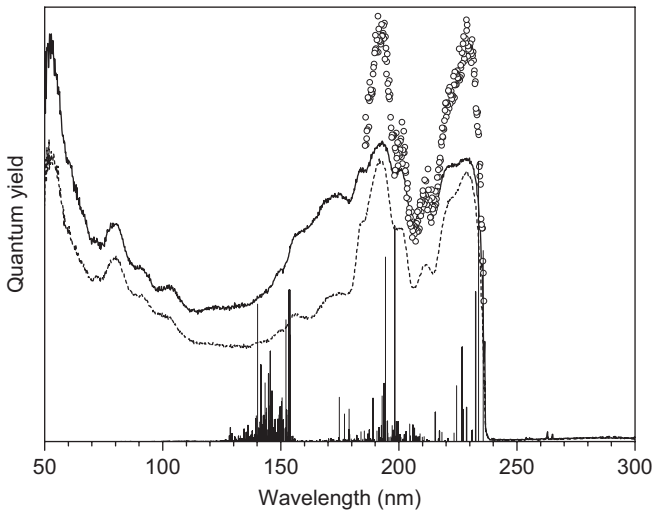

Fig. 6. Recorded excitation (at 8.5 K) and simulated absorption spectra for the $4f^3 \rightarrow 4f^2 5d$ transitions of Nd^{3+} in YAG. The solid and dashed curves are the experimental excitation spectra of Nd^{3+} f–f emission (at 400 nm) from YAG:Nd^{3+} (1.0 at%) and YAG:Nd^{3+} (0.5 at%), respectively, the open circles represent the experimental time-resolved excitation spectrum of the fast $4f^2 5d \rightarrow 4f^3$ emission (at 247 nm) from YAG:Nd^{3+} (0.5 at%). The vertical bars are the predicted positions of the zero-phonon lines with the heights proportional to the predicted intensities.

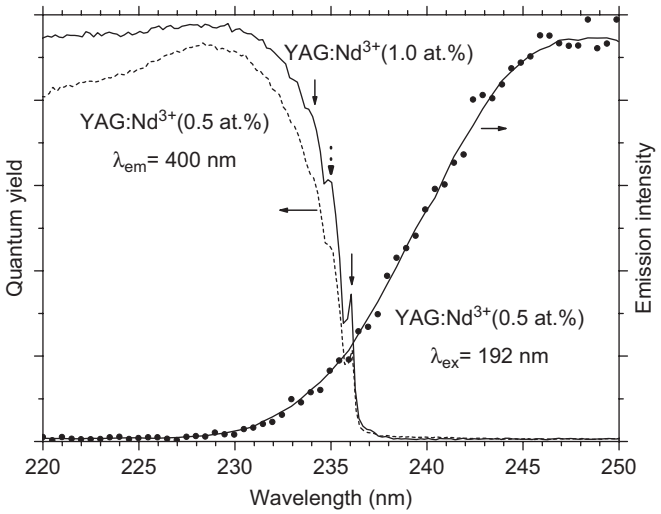

Fig. 7. Emission spectrum of YAG:Nd^{3+}(0.5%) (fast component; λ_{ex} 192 nm; dotted curve) and excitation spectra of Nd^{3+} f–f emission (λ_{em} 400 nm) from YAG:Nd^{3+}(0.5%) (dotted curve) and YAG:Nd^{3+}(1.0%) (solid curve) at 8.5 K near the excitation onset. The two vertical arrows show the zero-phonon line and the first member of the a_{1g} vibrational progression upon it. The dashed arrow designates the feature for which the origin is still under discussion (see text).

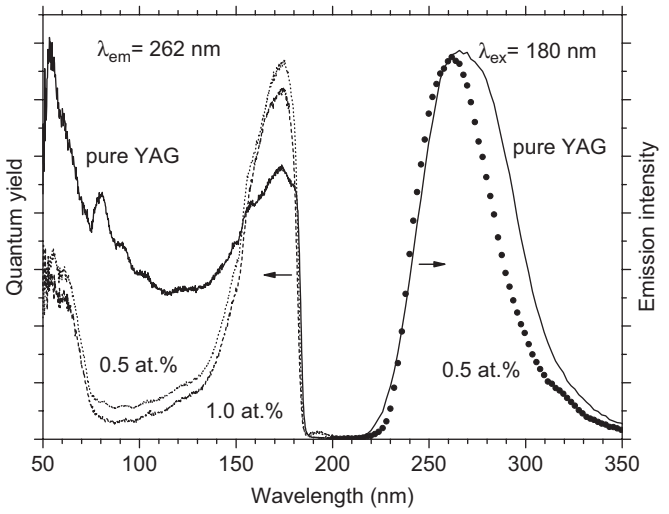

Fig. 8. 180 nm excited emission spectra of pure YAG (solid curve) and YAG:Nd^{3+}(0.5%) (dashed curve) and excitation spectra of intrinsic emission (λ_{em} 262 nm) from pure YAG (solid curve), YAG:Nd^{3+}(0.5 at%) (dotted curve) and YAG:Nd^{3+}(1.0 at%) (dashed curve) at 8.5 K.

structure of the $4f^25d$ bands between 240 nm and the edge of intrinsic absorption of the host at ~185 nm is well reproduced. One should also take into account that excitation spectrum well simulates the shape of absorption spectrum only in the case of very small concentration of absorbing impurity ions when $\alpha \cdot d \ll 1$ (α is absorption coefficient and d is the crystal thickness).

Excitation spectra of the 4.7 eV intrinsic emission in Nd^{3+}-doped YAG (Fig. 8) have the same thresholds at 6.7 eV (185 nm) as for neat YAG, but the emission intensity is strongly reduced at $hv > 8$ eV ($\lambda < 155$ nm), i.e. in the region of band-to-band transitions, and is increased again at $hv > 16.5$ eV ($\lambda < 75$ nm), where the increase of intrinsic emission intensity is observed also in pure YAG. It is supposed that under the band-to-band transitions the created electron–hole pairs can recombine either with each other (at regular sites or near some intrinsic defects) giving intrinsic emission (of STE or near-defect STE), or at the Nd^{3+} ions resulting in their f–f emission. Accordingly, it could be expected that the shape of the excitation spectrum of intrinsic emission from pure YAG in the region of band-to-band transitions will be similar to that of Nd^{3+} f–f emission from YAG:Nd^{3+} as is observed in our experimental spectra. In the region of band-to-band transitions, the charge carriers recombine mainly at Nd^{3+} giving intense Nd^{3+} emission, but less probably with each other resulting in weaker intrinsic emission in this spectral range for Nd^{3+}-doped YAG compared to pure YAG. Thus, in the region of band-to-band transitions a competition between the energy transfer from the host material to the intrinsic and the impurity (Nd^{3+}) centers is observed. Some energy transfer from intrinsic centers (STE) to Nd^{3+} also exists since Nd^{3+} f–f emission is efficiently excited in the region of excitonic absorption ($6.7 < hv < 8$ eV). This can be expected because the broad-band intrinsic emission has a good overlap in energy with the $^2F(2)_{5/2}$ emitting level of Nd^{3+} located at 4.68 eV (37,777 cm^{-1}). The increase of intensity of intrinsic and Nd^{3+} emission at $hv > 16.5$ eV is due to the effect of multiplication of electronic excitations when fast photoelectrons are able to create secondary excitons and/or secondary electron–hole pairs as discussed in Ref. [20].

4. Conclusions

The 192 nm excited luminescence spectra of 0.5 and 1 at% Nd^{3+}-doped YAG at 8.5 K are similar and show a fast emission component with the main peak at 248 nm (FWHM~30 nm) which corresponds to the transitions from the lowest $4f^25d$ state to the crystal-field levels of ^4I_J. The $4f^25d \rightarrow 4f^3$ emission, as well as the $4f^3 \rightarrow 4f^25d$ excitation spectra, are well simulated by crystal-field calculations. The 192 nm excited emission spectrum of YAG:Nd^{3+} also exhibits intraconfigurational $4f^3 \rightarrow 4f^3$ transitions from the $^2F(2)_{5/2}$ and $^4F_{3/2}$ multiplet terms. The experimentally derived energies of the $4f^3$ crystal-field levels from these emission spectra are in agreement with previous studies. As in the case of Cs_2NaYF_6:Nd^{3+} [17], the interconfigurational emission transitions to ^4I_J are more intense than to other multiplet terms, but the intraconfigurational transitions to ^4I_J from $^2F(2)_{5/2}$ are relatively weak.

Acknowledgments

PAT acknowledges financial support for this work under the Hong Kong University Research Grants Council Central Earmarked Research Grant City 102304. This work

was also supported by RFBR Grant 05-02-1730, Estonian Science Foundation (Grant 6538) and the European Community Research Infrastructure Action within the FP6 Program through the Contract RII3-CT-2004-506008 (IA-SFS). The authors acknowledge G. Stryganyuk for his assistance in the SUPERLUMI experiments.

References

[1] N.M. Khaidukov, M. Kirm, S.K. Lam, D. Lo, V.N. Makhov, G. Zimmerer, Opt. Commun. 184 (2000) 183.
[2] V.N. Makhov, N.Yu. Kirikova, M. Kirm, J.C. Krupa, P. Liblik, A. Lushchik, Ch. Lushchik, E. Negodin, G. Zimmerer, Nucl. Instr. Meth. A 486 (2002) 437.
[3] D. Wisniewski, S. Tavernier, P. Dorenbos, M. Wisniewska, A.J. Wojtowicz, P. Bruyndonckx, E. van Loef, C.W.E. van Eijk, L.A. Boatner, IEEE Trans. Nucl. Sci. 49 (2002) 937.
[4] D. Lo, V.N. Makhov, N.M. Khaidukov, J.C. Krupa, J.Y. Gesland, J. Lumin. 106 (2004) 15.
[5] A.F.H. Librantz, L. Gomes, S.L. Baldochi, I.M. Ranieri, G.E. Brito, J. Lumin. 121 (2006) 137.
[6] A. Collombet, Y. Guyot, M.F. Joubert, M. Laroche, J. Margerie, R. Moncorgé, E. Descroix, Phys. Rev. B 68 (2003) 035115.
[7] L. van Pieterson, M.F. Reid, R.T. Wegh, A. Meijerink, J. Lumin. 94–95 (2001) 79.
[8] T. Tomiki, Y. Isa, Y. Kadekawa, Y. Ganaha, N. Tokokawa, T. Miyazato, M. Miyazato, T. Kohatsu, H. Shimabukuro, J. Tamashiro, J. Phys. Soc. Jpn. 65 (1996) 1106.
[9] J.P. Hurrell, S.P.S. Porto, I.F. Chang, S.S. Mitra, R.P. Bauman, Phys. Rev. 173 (1968) 851.
[10] J.B. Gruber, D.K. Sardar, R.M. Yow, T.H. Allik, B. Zandi, J. Appl. Phys. 96 (2004) 3050.
[11] G.W. Burdick, C.K. Jayasankar, F.S. Richardson, M.F. Reid, Phys. Rev. B 50 (1994) 16309.
[12] G. Zimmerer, Nucl. Instr. Meth. A 308 (1991) 178.
[13] S. Geller, Z. für Krist. 125 (1967) 1.
[14] M.F. Reid, L. van Pieterson, R.T. Wegh, A. Meijerink, Phys. Rev. B 62 (2000) 14744.
[15] R.D. Cowan, The Theory of Atomic Structure and Spectra, University of California, Berkeley, 1981.
[16] T. Tomiki, T. Kohatsu, H. Shimabukuro, Y. Ganaha, J. Phys. Soc. Jpn. 61 (1992) 2382.
[17] P.A. Tanner, L. Ning, V.N. Makhov, N.M. Khaidukov, M. Kirm, J. Phys. Chem. B 110 (2006) 12113.
[18] L. van Pieterson, M.F. Reid, R.T. Wegh, S. Soverna, A. Meijerink, Phys. Rev. B 65 (2002) 045113.
[19] L. Ning, Y. Jiang, S. Xia, P.A. Tanner, J. Phys.: Condens. Matter 15 (2003) 7337.
[20] M. Kirm, A. Lushchik, Ch. Lushchik, G. Zimmerer, ECS Proc. 99–40 (2000) 113.
[21] V. Mürk, N. Yaroshevich, J. Phys.: Condens. Matter 7 (1995) 5857.
[22] J.A. Mares, W. Nie, G. Boulon, J. Lumin. 48&49 (1991) 227.